INTERNATIONAL JOURNAL FOR NUMERICAL METHODS IN FLUIDS
Int. J. Numer. Meth. Fluids 2002; **39**:161–187 (DOI: 10.1002/fld.219)

Refining the submesh strategy in the two-level finite element method: application to the advection–diffusion equation

Leopoldo P. Franca* and Feng-Nan Hwang

Department of Mathematics, University of Colorado at Denver, P.O. Box 173364, Campus Box 170, Denver, CO 80217-3364, U.S.A.

SUMMARY

We introduce a new submesh strategy for the two-level finite element method. The numerical results show that the new submesh is able to better capture the boundary layer which is caused by the choice of bubble functions. The effect of an improved approximation of the residual free bubbles is studied for the advective–diffusive equation. Copyright © 2002 John Wiley & Sons, Ltd.

KEY WORDS: finite element method; advection–diffusion; submesh strategy

1. INTRODUCTION

Herein, we approximate the advective–diffusive equation. The behavior of its solution depends on the magnitude of the velocity field and the diffusivity coefficient. These are part of the mesh-Peclet number definition, given as $Pe = [(|\boldsymbol{a}|h)/(2\kappa)]$, where $\boldsymbol{a}$ is the velocity field, h is the mesh size and κ is the diffusivity coefficient. When the Peclet number is large, we say that the numerical approximation is advective dominated; otherwise, it is diffusive dominated. In the finite element literature, it is well known that the standard Galerkin method using piecewise linears performs poorly for the advective dominated model. Spurious oscillations are frequently detected in the solution.

In order to overcome this difficulty, stabilized finite element methods have been introduced [1–3], and one version was denoted by the Galerkin least-squares method (GLS). The GLS method adds an 'artificial' term to the variational formulation. This additional term not only improves the numerical stability of the Galerkin method but also preserves good accuracy.

Another alternative is still to apply the standard Galerkin method to solve this problem by enriching polynomials with bubble functions. Herein we are interested in approximating the residual-free bubble (RFB) method using the Galerkin method. The bubble function is chosen so that the computed solution satisfies the original differential equation in the interior of each element and vanishes on the boundary of each element.

*Correspondence to: L. P. Franca, Department of Mathematics, University of Colorado at Denver, P.O. Box 173364, Campus Box 170, Denver, CO 80217-3364, U.S.A.

Received 19 June 2000
Revised 7 May 2001

Copyright © 2002 John Wiley & Sons, Ltd.

In Reference [4] a relationship is established between the stabilized finite element method and the Galerkin method using piecewise linears enriched with one bubble per element for the advective–diffusive model. Therein these two methods are shown to be equivalent for diffusive dominated models and appropriately defined element parameters h_k. Later, Brezzi *et al.* [5] proved the coercivity/stability inequality for a limiting case of the RFB method. Further progress has been made by Franca *et al.* [6], where they obtained the desired stability condition for positive but small diffusivity parameters under some hypotheses that the flow velocity is constant, the triangulation is regular, and the edges of the triangulation are bounded away from the direction of the flow.

A challenge for the RFB method is to determine the residual free bubble functions in a higher dimensional situation. The two-level finite element method (TLFEM) is a general framework to resolve this task. This method was first successfully used for solving the Helmholtz equation [7]. In Reference [6] the numerical results for the advection–diffusion problem showed that the TLFEM performed as well as the GLS and that there is no major qualitative difference between these two methods. The TLFEM consists of partitioning the mesh into submeshes, and an appropriate numerical method is then used to approximate the PDE's governing the residual-free bubble basis functions instead of solving analytically for the residual-free bubble functions. We can partition each mesh into different submeshes arbitrarily. For simplicity of implementation, uniform submeshes are considered first. However, due to the choice of bubble functions, there might be boundary layers near out-flow boundaries for the bubble shape functions. Therefore, it seems more appropriate to choose a new submesh which is able to capture the layer to produce more accurate approximate residual-free bubble shape functions.

The purpose of this work is to introduce a new nonuniform submesh depending on the direction of the flow, and compare numerical solutions of the TLFEM for advection–diffusion with uniform submeshes to see if we can get any improvement on the numerical solutions under the same global mesh.

The paper is organized as follows: in the next section, we review the residual-free bubble method for the general boundary value problem. Then, in Section 3, we discuss the two-level finite element method for the advective–diffusive equation derived from the RFB method; in Section 4 the algorithm for generating non-uniform submesh is developed. Finally, numerical results and conclusions are presented in Sections 5 and 6 respectively.

2. A REVIEW OF RFB FOR BOUNDARY VALUE PROBLEMS

Let us consider Ω to be an open bounded domain in R^2 with boundary $\partial\Omega$. For simplicity, we assume that $\partial\Omega$ is a polynomial curve in which case we say that Ω is a polynomial domain. (If $\partial\Omega$ is a curve, we can approximate it with a polynomial).

First, we consider the general boundary value problem

$$\begin{cases} Lu = f & \text{in } \Omega \\ u = 0 & \text{on } \partial\Omega \end{cases} \tag{1}$$

where L is a linear differential operator, e.g. L may be the advective–diffusive operator, u is the unknown scalar function and f is a given source function. We also assume that this problem is well posed.

Copyright © 2002 John Wiley & Sons, Ltd.

The abstract variational formulation of Equation (1) is as follows: find a scalar variable $u \in V$ such that

$$a(u, v) = (f, v) \quad \forall v \in V \tag{2}$$

where V is a Hilbert space, $a(\cdot, \cdot)$ is a bilinear form from $V \times V$ to R and $(\cdot, \cdot)$ is the usual scalar product in $L^2(\Omega)$.

To specify the standard Galerkin finite element for Equation (1), we partition the domain Ω into several pieces K (e.g. triangles, quadrilaterals etc.) in the standard way, which forbids overlapping or any vertex on the edge of a neighboring element, and so on. Thus,

$$\Omega = \bigcup_{K \in T_h} K = K_1 \cup K_2 \cup \cdots \cup K_m \tag{3}$$

where T_h is a partition of Ω.

We introduce the mesh parameter

$$h = \max_{K \in T_h} \operatorname{diam}(K), \quad \operatorname{diam}(K) = \text{diameter of } K \tag{4}$$

We now define V_h as a finite-dimensional space, which is a subspace of V.

Then the standard Galerkin finite element method is: find $u_h \in V_h$ such that

$$a(u_h, v_h) = (f, v_h) \quad \forall v_h \in V_h \tag{5}$$

Now, we decompose the space V_h such that $V_h = V_1 + B$, where V_1 is the space of continuous piecewise linear or bilinear polynomials and B is the space of residual-free bubbles. We will define the space B explicitly later.

Then every $u_h \in V_h$ can be written in the form of $u_h = u_1 + u_b$, where $u_1 \in V_1$ and $u_b \in B$. For the residual-free bubble space, we require the bubble component u_b of each u_h to vanish on ∂K of each K and require each u_h to satisfy the original differential equations strongly, i.e.

$$L(u_1 + u_b) = f \quad \text{in } K \tag{6}$$

or

$$Lu_b = -(Lu_1 - f) \quad \text{in } K \tag{7}$$

subject to zero Dirichlet boundary condition on the element boundary, i.e.

$$u_b = 0 \quad \text{on } \partial K \tag{8}$$

By the classical static condensation procedure, first we set $v_h = v_b$ in K and $v_h = 0$ elsewhere in Equation (5) to have

$$a(u_1 + u_b, v_b)_K = (f, v_b)_K \quad \forall v_b \in B \tag{9}$$

where $a(\cdot, \cdot)_K$ and $(\cdot, \cdot)_K$ indicate that integration is restricted to the element K.

Then, taking $v_h = v_1$ in Equation (5), we obtain

$$a(u_h, v_1) = (f, v_1) \tag{10}$$

Copyright © 2002 John Wiley & Sons, Ltd.

or

$$a(u_1 + u_b, v_1) = (f, v_1) \tag{11}$$

The formulation of Equation (9) is automatically true due to our choice of bubble functions. In fact, this equation is also the variational formulation of Equation (6) using v_b as test function restricted to each element K. Furthermore, Equation (11) is the method used to compute an improved bilinear or linear approximation due to the residual-free bubbles effect. To find the residual-free bubble part of the solution, we need to solve Equation (5) which depends on the linear part of the solution u_1. Instead, bubble shape functions with i varying from one to the number of element nodes (Nen) can be obtained by the following auxiliary problems:

(i) for each $i = 1, 2, \ldots, Nen$, find ϕ_i
such that

$$L\phi_i = -L\psi_i \quad \text{in } K \tag{12}$$

$$\phi_i = 0 \quad \text{on } \partial K \tag{13}$$

where the ψ_i are local basis function for u_1 and

(ii) find ϕ_f such that

$$L\phi_f = f \quad \text{in } K \tag{14}$$

$$\phi_f = 0 \quad \text{on } \partial K \tag{15}$$

Thus if

$$u_1 = \sum_{i=1}^{Nen} c_i \phi_i \tag{16}$$

then

$$u_b = \sum_{i=1}^{Nen} c_i \psi_i + \psi_f \tag{17}$$

with the same coefficient c_i.

Furthermore, we have the following representation:

$$u_{h,K} = \sum_{i=1}^{Nen} c_i(\psi_i + \phi_i) + \phi_f \tag{18}$$

Hence, we can define the residual-free bubble space B_K as

$$B_K = \text{span}\{\phi_1, \ldots, \phi_{Nen}, \phi_f\} \tag{19}$$

and

$$B = \sum_{K \in T_h} B_K \tag{20}$$

Copyright © 2002 John Wiley & Sons, Ltd.

Therefore, we can restate the RFB method for general boundary value problem as follows:

$$\begin{cases} \text{Find } u_h = u_1 + u_b \in V_h = V_1 + B \quad \text{such that} \\ \quad a(u_h, v_1) = (f, v_1) \quad \forall v_1 \in V_1 \\ \quad\quad a(u_h, v_b)_K = (f, v_b)_K \quad \forall K \in T_h \text{ and } v_b \in B_K \end{cases} \tag{21}$$

or we can eliminate u_b in Equation (21) and obtain an equation which only involves u_1:

$$\begin{cases} \text{Find} \quad u_1 \in V_1 \quad \text{such that} \\ \quad a(u_1, v_1) + \sum_{K \in T_h} a(u_b, v_1)_K = (f, v_1) \quad \forall v_1 \in V_1 \end{cases} \tag{22}$$

To get u_b as a function of u_1 and f requires solving Equations (12)–(15), which is as complicated as solving the original differential equation, unless we have special cases such as rectangular elements such that we can employ classical analytical tools to get an exact solution within each element. Henceforth our strategy is to approximate the bubble shape functions $\psi_{i,K}$ and $\psi_{f,K}$ by another appropriate finite element method. In other words, at the global level we use the standard Galerkin method with piecewise linears for the original problem. At the element level, we partition each element into a finer submesh and then utilize non-standard finite element methods to solve the bubble problems. This is why we called this method a two-level finite element method (TLFEM). In this work, we apply the improved Unusual Stabilized Finite Element Method (the improved US-FEM) [8] to approximate the bubble shape functions. Because we use linears at this level, GLS or SUPG can also be used with the same stability parameter as in Reference [8], to get identical results. We discuss TLFEM in more detail in the next section.

3. THE TLFEM FOR THE ADVECTIVE–DIFFUSIVE PROBLEM

In the present section we develop the TLFEM based on the RFB method and discuss its application to the advective–diffusive problem. This approach is general, and can be applied to an arbitrarily shaped domain without any difficulty. For the advective–diffusive problem, we set

$$L = -\kappa\Delta + \boldsymbol{a} \cdot \nabla \tag{23}$$

Here $\boldsymbol{a}$ is the given velocity field, assumed to be constant in each element, and κ is the given positive constant diffusivity coefficient. We are interested in the advective-dominated case, i.e. when $\kappa \ll |\boldsymbol{a}|$. The associated bilinear form is

$$a(u, v) = \kappa(\nabla u, \nabla v) + (\boldsymbol{a} \cdot \nabla u, v) \tag{24}$$

At the global level, we rewrite Equation (11) for the advective–diffusive problem:

$$\kappa(\nabla u_1, \nabla v_1) + \kappa(\nabla u_b, \nabla v_1) + (\boldsymbol{a} \cdot \nabla u_1, v_1) + (\boldsymbol{a} \cdot \nabla u_b, v_1) = (f, v_1) \tag{25}$$

Copyright © 2002 John Wiley & Sons, Ltd.

Then, let us consider the second term above:

$$\begin{aligned}\kappa(\nabla u_b, \nabla v_1) &= \sum_K \kappa(\nabla u_b, \nabla v_1)_K \\ &= \sum_K \kappa \int_K \nabla u_b \cdot \nabla v_1 \, \mathrm{d}x \\ &= \sum_K \left(\kappa \int_{\partial K} u_b \nabla v_1 \cdot \boldsymbol{n} \, \mathrm{d}s - \kappa \int_K u_b \Delta v_1 \, \mathrm{d}x \right)\end{aligned}$$

where $\boldsymbol{n}$ is a unit normal vector. The last equality is obtained by integration-by-parts. Since the residual-free bubble function u_b's are zero on element boundaries and v_1 is bilinear inside rectangular elements, we conclude that $\kappa(\nabla u_b, \nabla v_1) = 0$.

Therefore, Equation (25) simplifies to

$$\kappa(\nabla u_1, \nabla v_1) + (\boldsymbol{a} \nabla u_1, v_1) + (\boldsymbol{a} \cdot \nabla u_b, v_1) = (f, v_1) \tag{26}$$

Substituting Equation (18) into Equation (26) and setting $v_1 = \psi_j$ enables us to write the matrix problem: find the coefficient c_i's such that

$$\sum_i c_i [(\kappa \nabla \psi_i, \nabla \psi_j) + (\boldsymbol{a} \cdot \nabla \psi_i, \psi_j) + (\boldsymbol{a} \cdot \nabla \phi_i, \psi_j)] = (f, \psi_j) - (\boldsymbol{a} \cdot \nabla \phi_f, \psi_j) \tag{27}$$

i runs over all unknown interior nodes in the elements, say through N.

At the local element level, Equations (12)–(15) for the advective–diffusive problem reads:

(i) for $i = 1, \ldots, Nen$,

$$\boldsymbol{a} \cdot \nabla \phi_i - \kappa \Delta \phi_i = -\boldsymbol{a} \cdot \nabla \psi_i \quad \text{in } K \tag{28}$$

$$\phi_i = 0 \quad \text{on } \partial K \tag{29}$$

(ii)

$$\boldsymbol{a} \cdot \nabla \phi_f - \kappa \Delta \phi_f = f \quad \text{in } K \tag{30}$$

$$\phi_f = 0 \quad \text{on } \partial K \tag{31}$$

For advective dominated regimes we expect outflow boundary layers for these bubble shape functions. Our strategy is to use the nonuniform submesh which is more refined near the outflow boundaries depending on the direction of the velocity field. Figure 1 illustrates this idea.

We begin to approximate residual-free bubble shape functions by partitioning each element K into the coarse submesh K^* (a mesh defined for each element) with diameter h^* and denote by ψ_i^* the basis function for a piecewise linear interpolation on the submesh.

Therefore, our unknown bubble basis function can be approximated by

$$\phi_i^{h^*} = \sum_l^{N^*} c_l^{(i)} \psi_l^* \tag{32}$$

Copyright © 2002 John Wiley & Sons, Ltd.

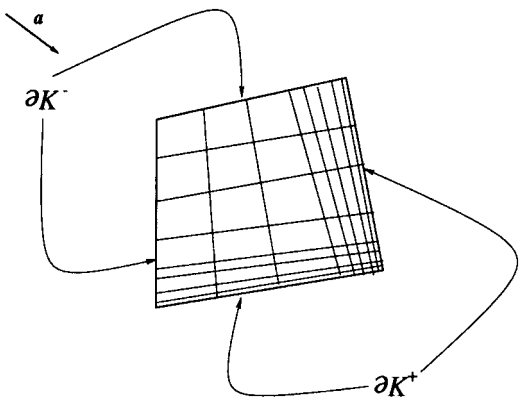

Figure 1. Submesh refines on outflow boundaries.

Here N^* is the number of all unknown interior nodes in the submesh. The index i refers to specific bubble function that we are trying to compute.

Similarly, under the presence of a source term f, the other bubble shape function is given by:

$$\phi_f^{h^*} = \sum_l^{N^*} c_l^f \psi_l^* \tag{33}$$

Then we can formulate the improved US-FEM [8] for the case in which the reactive term is equal to zero in the matrix formulation for Equations (28) and (29) as: for each i (from 1 to Nen) find $c_l^{(i)}$, such that

$$\begin{aligned}\sum_l c_l^{(i)}[(\boldsymbol{a}\cdot\nabla\psi_l^*,\psi_m^*)+(\kappa\nabla\psi_l^*,\nabla\psi_m^*)+(\boldsymbol{a}\cdot\nabla\psi_l^*,\tau a\cdot\psi_m^*)]\\ =(-\boldsymbol{a}\cdot\nabla\psi_{i,K},\psi_m^*+\tau\boldsymbol{a}\cdot\nabla\psi_m^*)\end{aligned} \tag{34}$$

In addition, the matrix formulation for Equations (30) and (31) is given by: find c_l^f, such that

$$\sum_l c_l^f[(\boldsymbol{a}\cdot\nabla\psi_l^*,\psi_m^*)+(\kappa\nabla\psi_l^*,\nabla\psi_m^*)+(\boldsymbol{a}\cdot\nabla\psi_l^*,\tau\boldsymbol{a}\cdot\psi_m^*)]=(f,\psi_m^*+\tau\boldsymbol{a}\cdot\nabla\psi_m^*) \tag{35}$$

We use the stability τ suggested in Reference [8] as

$$\tau(x,Pe_K(x))=\frac{h_K^{*2}}{6\kappa+6\kappa\xi(Pe_K(x))} \tag{36}$$

$$Pe_K(x)=\frac{|\boldsymbol{a}(x)|_2 h_K^*}{3\kappa(x)} \tag{37}$$

Copyright © 2002 John Wiley & Sons, Ltd.

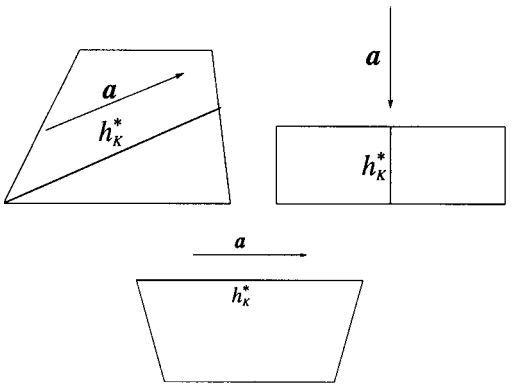

Figure 2. The element parameter computation.

$$\xi(x) = \begin{cases} 1, & \text{if } 0 \leqslant x < 1 \\ x, & \text{if } x \geqslant 1 \end{cases} \tag{38}$$

$$|\boldsymbol{a}(x)|_2 = \sum_{i=1}^{2} (|a_i(x)^2|)^{1/2} \tag{39}$$

And the element parameter h_K^* is computed by using the largest streamline distance of elements. See Figure 2.

Once the constants $c_l^{(i)}$ and c_l^f are determined, we substitute them into Equations (32) and (33) respectively to get the approximate residual basis functions $\phi_l^{h^*}$ and $\phi_f^{h^*}$.

For a practical problem such as the flow over an airfoil or an automobile, the direction of the flow varies element-wise. Therefore, it is necessary for us to design a subroutine in our computer program to generate the nonuniform submesh automatically. Before proceeding to discuss the algorithm for a submesh generator, let us list all combinations of outflow and inflow boundary segments of elements and indicate the submeshes which are used for each different case. Other permutations are not listed, since they are covered by all combinations listed in Figure 3.

4. THE ALGORITHM FOR THE NONUNIFORM SUBMESH GENERATOR

We begin our study of this subject with an algorithm for meshes in one dimension and proceed to generalize to more sophisticated nonuniform irregular mesh generation schemes for the two-dimensional case. An algorithm for a uniform mesh on interval (a, b) can be written as:

STEP 1 Set $h = \frac{1}{n}$: $n =$ number of elements

STEP 2 For $i = 1, \ldots, n$: Set $\alpha_i = (i-1)h$.

Then $\bar{\xi}_i = a + (b-a)g_1(\alpha_i)$ defines the node location, where $g_1(\alpha) = \alpha$.

Copyright © 2002 John Wiley & Sons, Ltd.

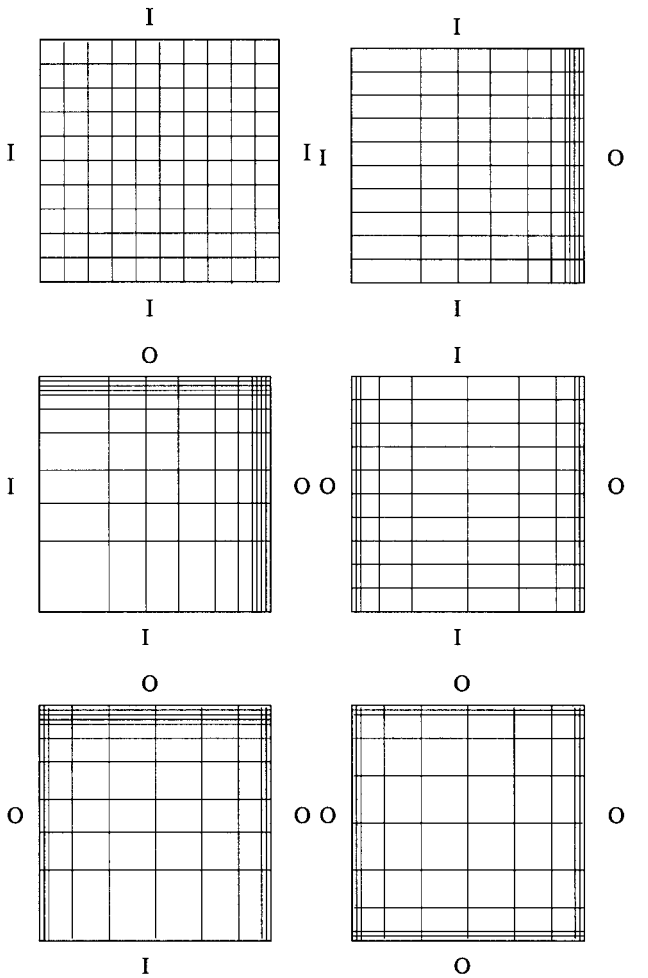

Figure 3. Submesh used for different cases: 'I' indicates 'inflow' boundary and 'O' indicates 'outflow' boundary.

For our nonuniform mesh, we can define two mappings:

$$\xi = g_2(\alpha) = \alpha^2 \tag{40}$$

$$\xi = g_3(\alpha) = (1-\alpha)^2 \tag{41}$$

Replacing $g_1(\alpha)$ by $g_2(\alpha)$ in **STEP 2**, the mapping $g_2(\alpha)$ will take the uniform mesh in α to a quadratically graded mesh from left to right in ξ. (See Figure 4.) Conversely, the mapping $g_3(\alpha)$ will take the uniform mesh in α to a quadratically graded mesh from right to left in ξ, if we rewrite **STEP 2** as: For $i = 1, \ldots, n$:

Set $\alpha_i = (i-1)h$. Then $\bar{\xi}_i = b - (b-a)g_3(\alpha_i)$ defined the node location.

Copyright © 2002 John Wiley & Sons, Ltd.

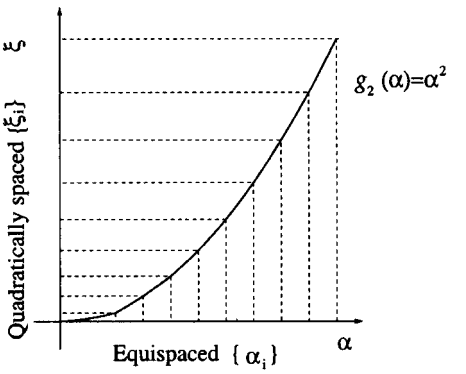

Figure 4. Mesh grading from left to right: a quadratic transformation.

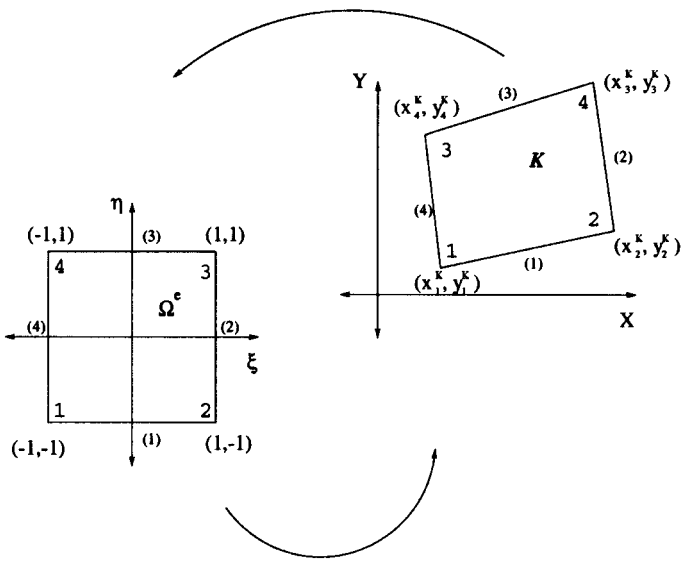

Figure 5. Local node and side ordering.

Or if we wish to produce a mesh that is graded into both ends $\bar{\xi} = a$ and $\bar{\xi} = b$, we can combine these two mappings $g_2(\alpha)$ and $g_3(\alpha)$ and define

$$g_4(\alpha) = \begin{cases} \alpha^2, & 0 \leqslant \alpha < 0.5 \\ (1-\alpha)^2, & 0.5 \leqslant \alpha \leqslant 1 \end{cases} \tag{42}$$

Now, let us generalize this idea to a two-dimensional irregular mesh.

Let K be a quadrilateral element defined by locations of its four nodal points x_a^K, $a = 1, \ldots, 4$ in the physical domain R^2 and $\Omega^e = [0,1] \times [0,1]$ be a corresponding biunit square in the computational domain. The nodal points and sides of elements either in the physical or the computational domain are labeled in ascending counterclockwise direction. See Figure 5.

Copyright © 2002 John Wiley & Sons, Ltd.

The coordinates of a point (ξ,η) in the biunit square Ω^e are related to the coordinates of a point (x,y) in K by the transformations:

$$x(\xi,\eta)=\sum_{a=1}^{4} N_a(\xi,\eta)x_a^e \tag{43}$$

$$y(\xi,\eta)=\sum_{a=1}^{4} N_a(\xi,\eta)y_a^e \tag{44}$$

where

$$N_1(\xi,\eta)=\frac{1}{4}(1-\xi)(1-\eta),\quad N_2(\xi,\eta)=\frac{1}{4}(1+\xi)(1-\eta)$$

$$N_3(\xi,\eta)=\frac{1}{4}(1+\xi)(1+\eta),\quad N_4(\xi,\eta)=\frac{1}{4}(1-\xi)(1+\eta)$$

Let us introduce some notations used in the algorithm.

(i) Nsd: number of space dimensions (Here $Nsd=2$)
(ii) N^*es: number of elements for submesh ($N^*es=n\times m$)
(iii) N^*np: number of nodal points for submesh
(iv) a: local node number for mesh ($1\leqslant a\leqslant 4$)
(v) a^*: local node number for submesh ($1\leqslant a^*\leqslant 4$)
(vi) A^* global node number for submesh ($1\leqslant A^*\leqslant N^*np$)
(vii) i: spatial index ($1\leqslant i\leqslant Nsd$)
(viii) e^*: element number for submesh ($1\leqslant i^*\leqslant N^*es$)
(ix) $\mathrm{ID}^*(A^*)$: destination matrix for submesh
(x) $\mathrm{IEN}^*(a^*,e^*)$: location matrix for submesh
(xi) $x^K(a,i)$: coordinates of nodal points for mesh
(xii) $x^{K^*}(A^*,i)$ coordinates of global node number for submesh.

Similarly to the global level, three data processing arrays, $\mathrm{IEN}^*,\mathrm{ID}^*$ and $x^{K^*}(A^*,i^*)$ are needed as input data. For more detailed discussion see Reference [9].

Here is the algorithm for the irregular mesh generator:

INPUT: $x^K(a,i),m,n$

OUTPUT: $\mathrm{ID}^*(\mathrm{A}^*),\mathrm{LM}^*(\mathrm{a}^*,\mathrm{e}^*),x^{K^*}(A^*,i)$

STEP 1 Determine whether each boundary of element K is 'inflow' or 'outflow' by the definition and then properly label each corresponding segment of the biunit square Ω^e.

STEP 2 Set $h=\frac{2}{n},\ k=\frac{2}{m}$.

STEP 3 Compute the horizontal coordinates of the submesh for the biunit square Ω^e:

Define the following mapping:

$$f_1(x)=x^3 \tag{45}$$

$$f_2(x)=(1-x)^3 \tag{46}$$

$$f_3(x)=x \tag{47}$$

Note: The domains of these three functions are $[0,1]$.

Copyright © 2002 John Wiley & Sons, Ltd.

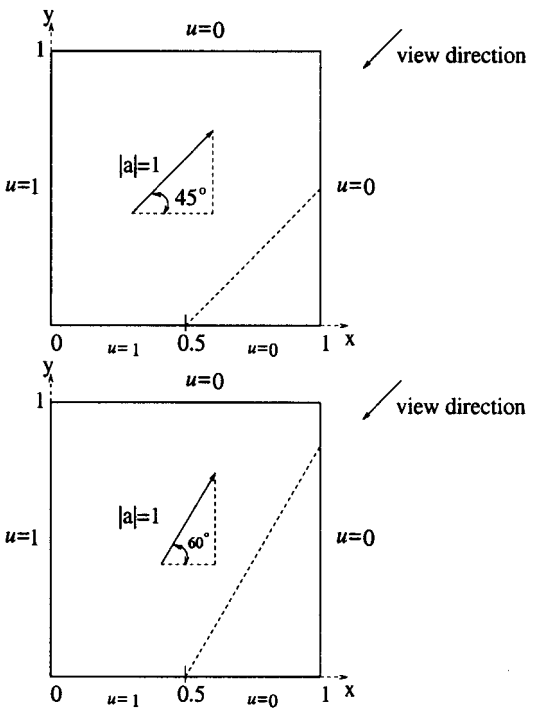

Figure 6. Domain for skew convection problems with two different velocity fields.

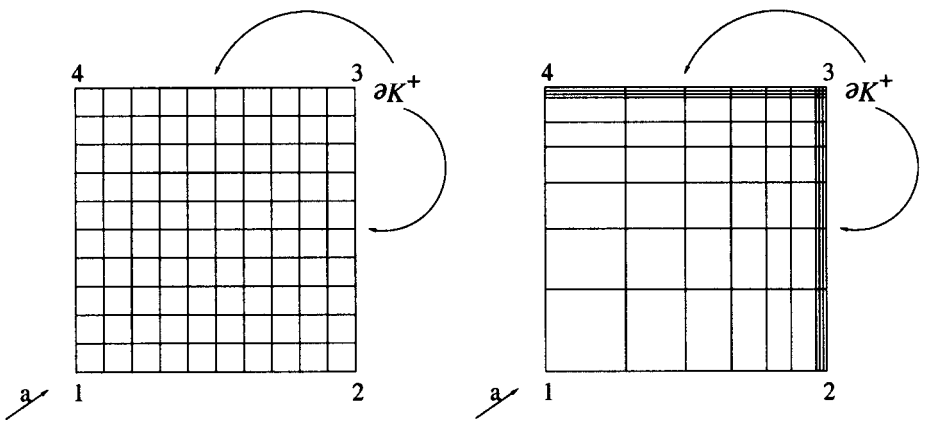

Figure 7. Two different 10×10 submeshes used for TLFEM: uniform (left) and nonuniform (right).

Case 1: Side (2) and Side (4) are both 'inflow' boundary segments
For $i = 1, \ldots, n+1$:
Set $\alpha_i = (i-1)h$. Then $\bar{\xi}_i = -1 + 2f_3(\alpha_i)$;

Copyright © 2002 John Wiley & Sons, Ltd.

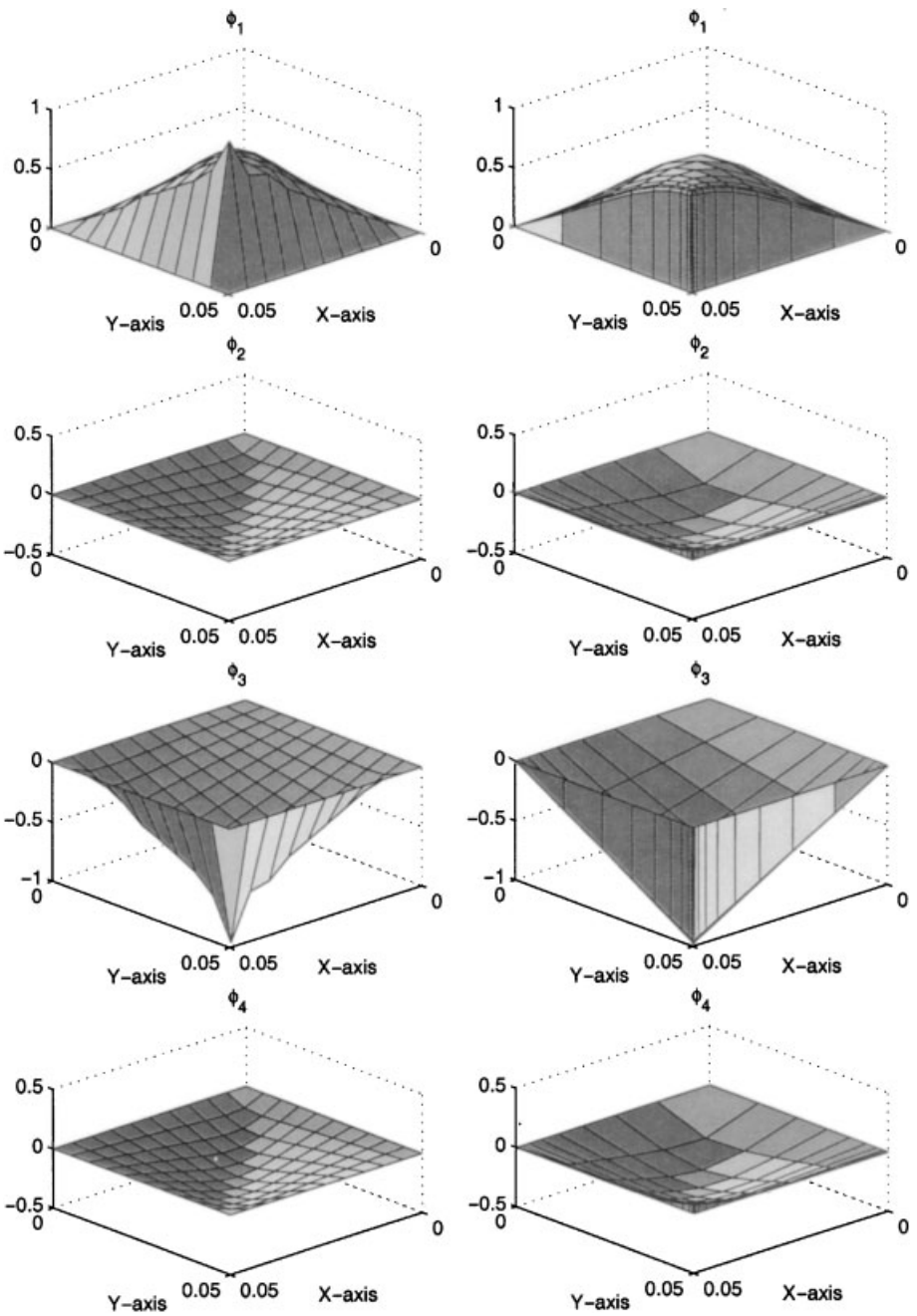

Figure 8. Comparison of bubble shape functions by using two different submeshes for the 45° problem: uniform (left) and nonuniform (right).

Copyright © 2002 John Wiley & Sons, Ltd.

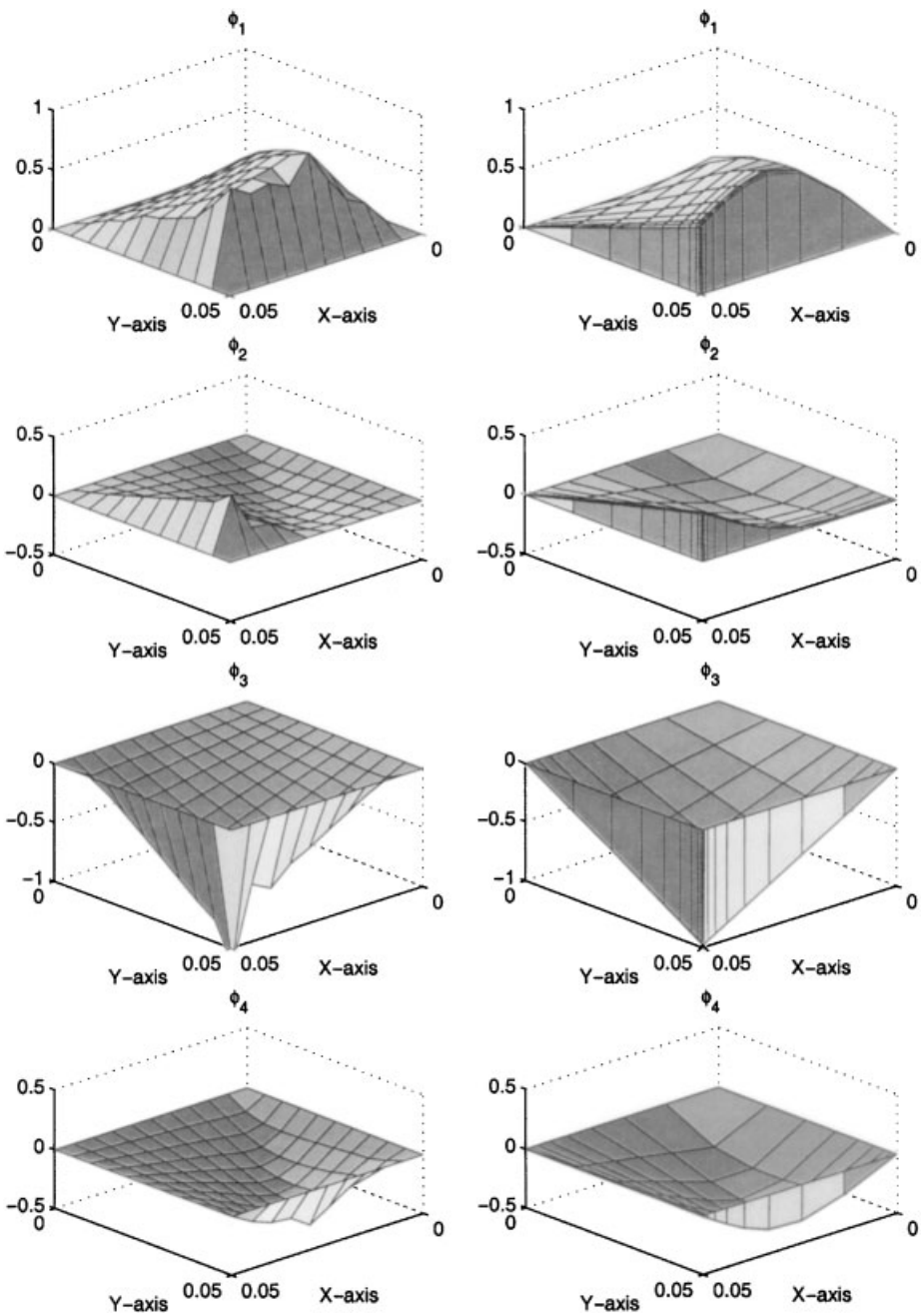

Figure 9. Comparison of bubble shape functions by using two different submeshes for the 60° problem: uniform (left) and nonuniform (right).

Copyright © 2002 John Wiley & Sons, Ltd.

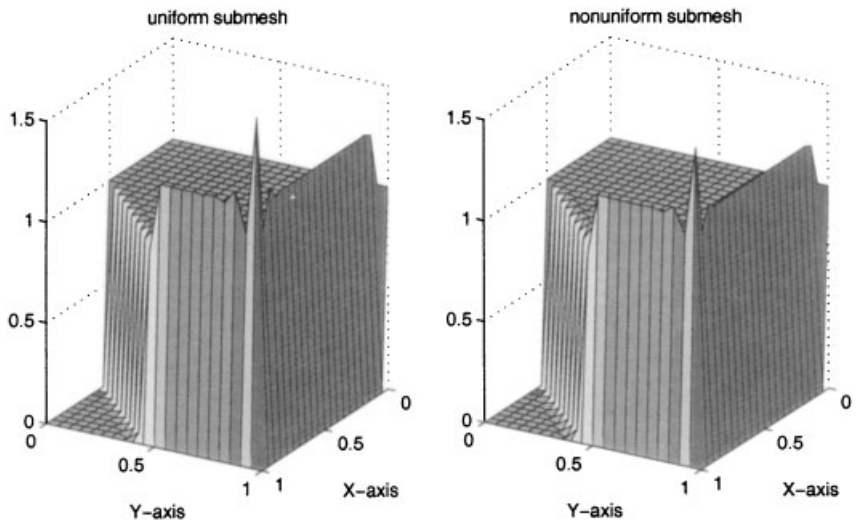

Figure 10. Comparison of TLFEM solutions by using two different submeshes for the 45° problem: uniform (left) and nonuniform (right).

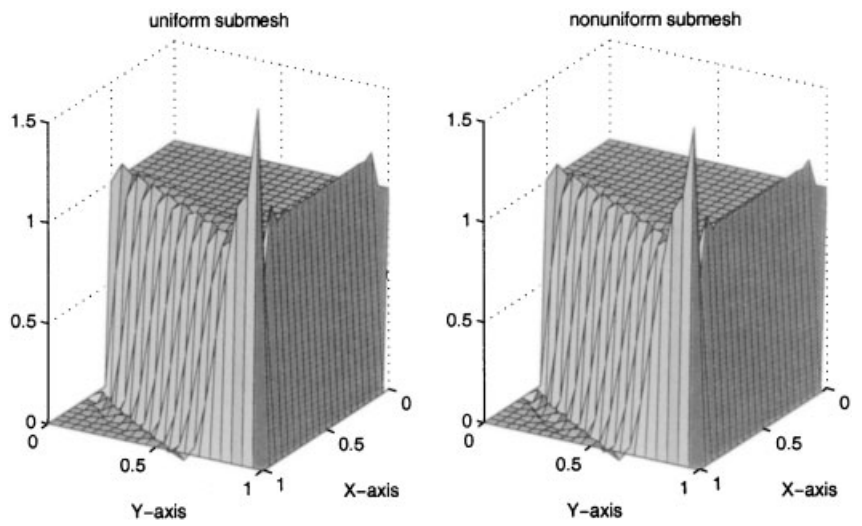

Figure 11. Comparison of TLFEM solutions by using two different submeshes for the 60° problem: uniform (left) and nonuniform (right).

Case 2: Side (2) and Side (4) are both 'outflow' boundary segments
For $i = 1, \ldots, [n/2]$:
Set $\alpha_i = (i-1)h$. Then $\bar{\xi}_i = -1 + 2f_1(\alpha_i)$ and
for $i = [n/2+1], \ldots, n+1$:
Set $\alpha_i = (i-1)h$. Then $\bar{\xi}_i = 1 - 2f_2(\alpha_i)$;

Copyright © 2002 John Wiley & Sons, Ltd.

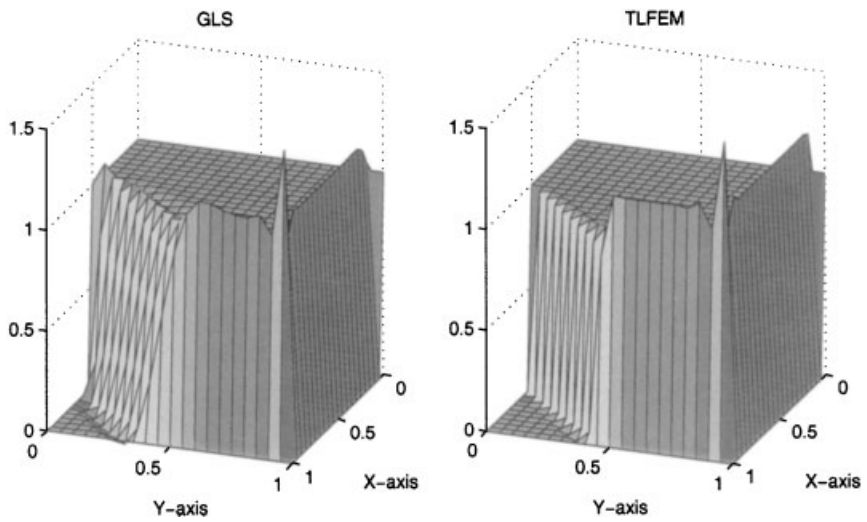

Figure 12. Comparison of GLS and TLFEM solutions for the 45° problem: GLS (left) and TLFEM (right).

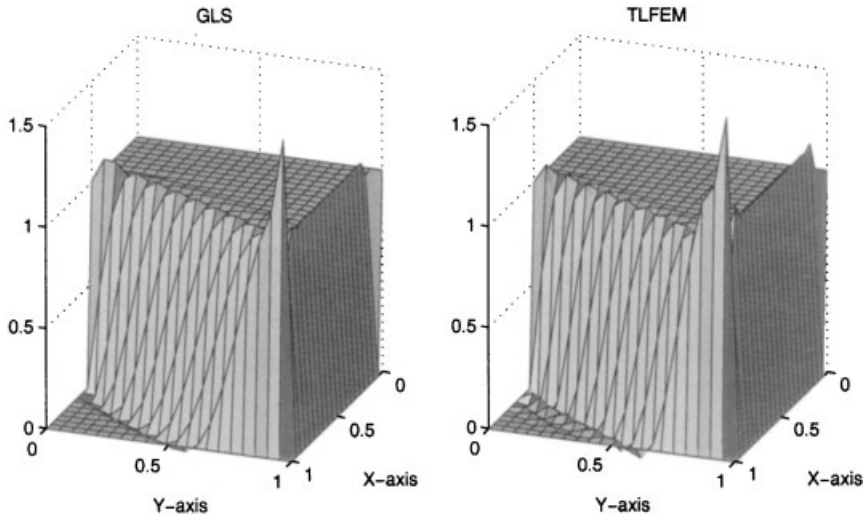

Figure 13. Comparison of GLS and TLFEM solutions for the 60° problem: GLS (left) and TLFEM (right).

Case 3: Side (2) is 'inflow' and Side (4) is 'outflow' boundary segment
For $i=1,\ldots,n$:
Set $\alpha_i=(i-1)h$. Then $\bar{\xi}_i=-1+2f_1(\alpha_i)$;

Copyright © 2002 John Wiley & Sons, Ltd.

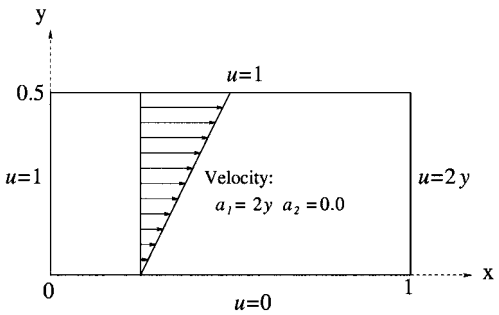

Figure 14. Problem statement for the thermal boundary layer problem.

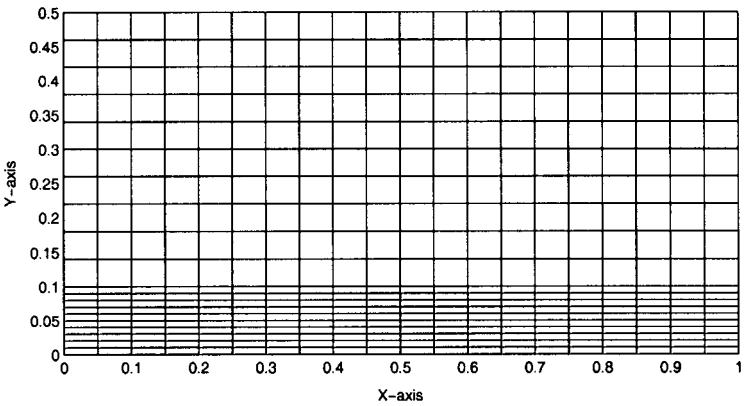

Figure 15. Mesh used for the thermal boundary layer problem.

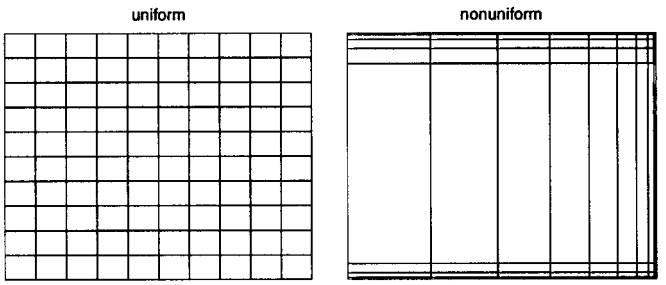

Figure 16. Submesh used for the thermal boundary layer problem.

Case 4: Side (2) is 'outflow' and Side (4) is 'inflow' boundary segment
For $i=1,\ldots,n$:
Set $\alpha_i=(i-1)h$. Then $\bar{\xi}_i=1-2f_2(\alpha_i)$;

STEP 4 Compute the vertical coordinates of the submesh for biunit square Ω^e.
Similar to **STEP 3**, now we consider Side (1) and Side (3) of Ω^e.

Copyright © 2002 John Wiley & Sons, Ltd.

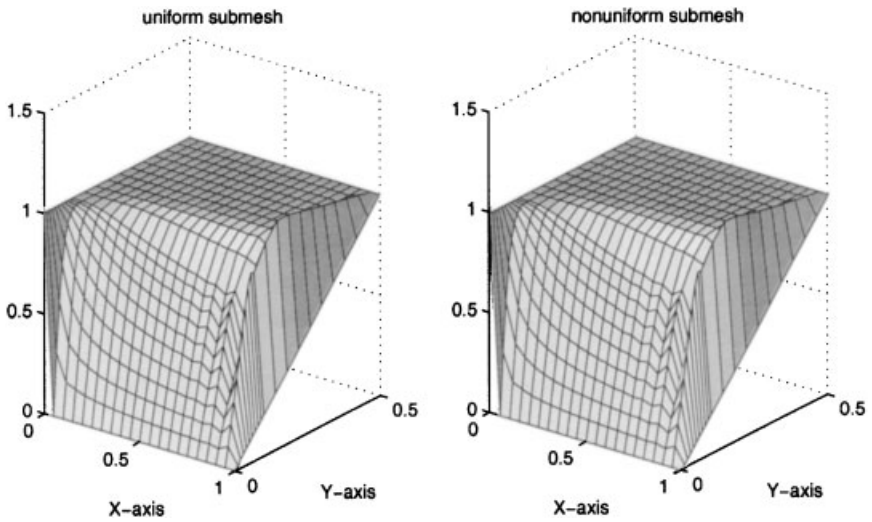

Figure 17. Bubble shape functions for the diffusive dominated case: uniform submesh (left) and nonuniform submesh (right).

STEP 5 Set $\mathrm{ID}^*(A^*)=0$ on the boundary nodes and $eq=1$;
STEP 6 For $i=1,\ldots,n$; $j=1,\ldots,m$: do **STEP 7**–**STEP 10**
STEP 7 Construct $\mathrm{ID}^*(A^*)$ for submesh
Set $A^*=(i-1)*(n+1)+j$, $A^*\equiv(i,j)$;
If $\mathrm{ID}^*(A^*)\neq 0$ then $\mathrm{ID}(A^*)=eq$ and set $eq=eq+1$;
STEP 8 Construct $\mathrm{IEN}^*(a^*,e^*)$ for submesh:
Set $e^*=(i-1)*(n+1)+j$;
Then $\mathrm{IEN}^*(1,e^*)=A^*$, $\mathrm{IEN}^*(2,e^*)=A^*+1$,
$\mathrm{IEN}^*(3,e^*)=A^*+n+2$, $\mathrm{IEN}^*(4,e^*)=A^*+n+1$.
STEP 9 Compute the coordinate of node points (node A^*):

$$\begin{aligned}\xi_{A^*} &= \bar{\xi}_i \\ \eta_{A^*} &= \bar{\eta}_j\end{aligned} \tag{48}$$

STEP 10 Map the coordinates of node points (ξ_{A^*},η_{A^*}) from the computational domain to the physical domain by the transformations of Equations (43) and (44).

5. NUMERICAL RESULTS

In this section, we report three series of experiments for the advection–diffusion problem with TLFEM using the new non-uniform submesh introduced in the previous section. In the following numerical results, we illustrate the applicability of the method for singularly perturbed problems, i.e. for small values of the diffusivity κ compared with the advection field.

Copyright © 2002 John Wiley & Sons, Ltd.

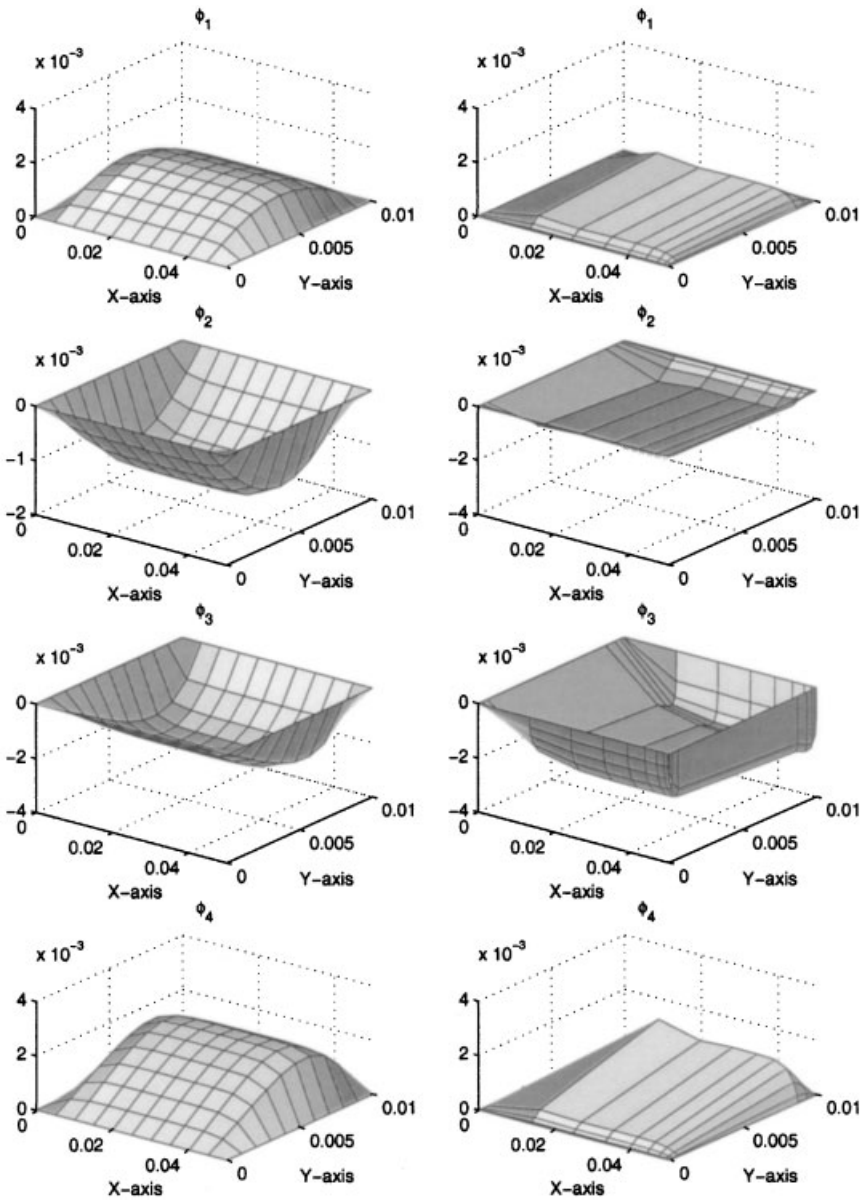

Figure 18. Bubble shape functions for the advective dominated case: uniform submesh (left) and nonuniform submesh (right).

5.1. A problem with discontinuous boundary condition

In the first two experiments, let us consider a unit square domain Ω with inflow discontinuous boundary values at $(0.5, 0)$. The diffusivity is $\kappa = 10^{-6}$, and we will test our methods for two

Copyright © 2002 John Wiley & Sons, Ltd.

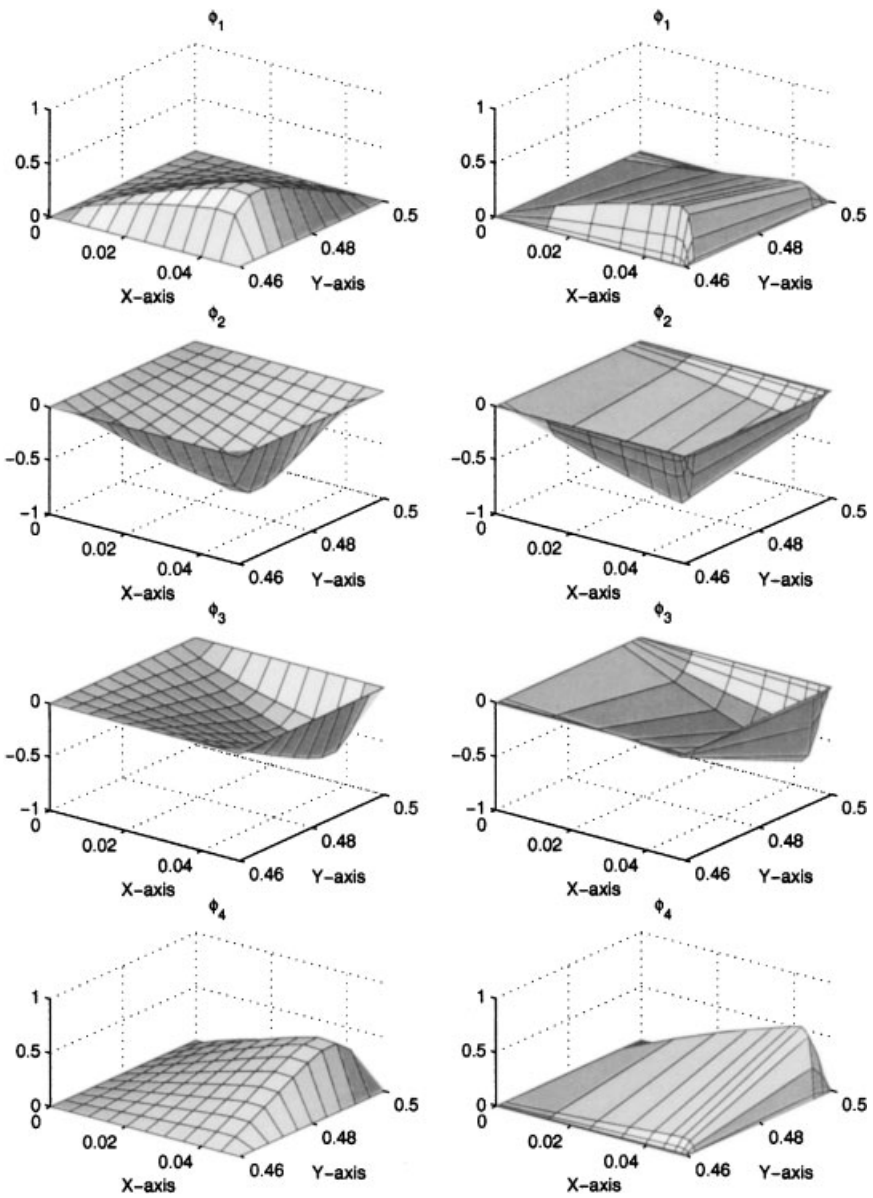

Figure 19. Comparison of TLFEM solutions using two different submeshes.

different angles of the uniform velocity field of size one with the horizontal axis. The first case is 45° and the second one is 60° (see Figure 6 for problem statements).

In these problems, a discontinuous data at the inflow boundary is propagated into the domain which causes an internal layer along the characteristic of the problem starting at point $(0.5, 0)$. In addition, the problems are subjected to homogeneous Dirichlet boundary conditions at the outflow boundary which create the outflow boundaries.

Copyright © 2002 John Wiley & Sons, Ltd.

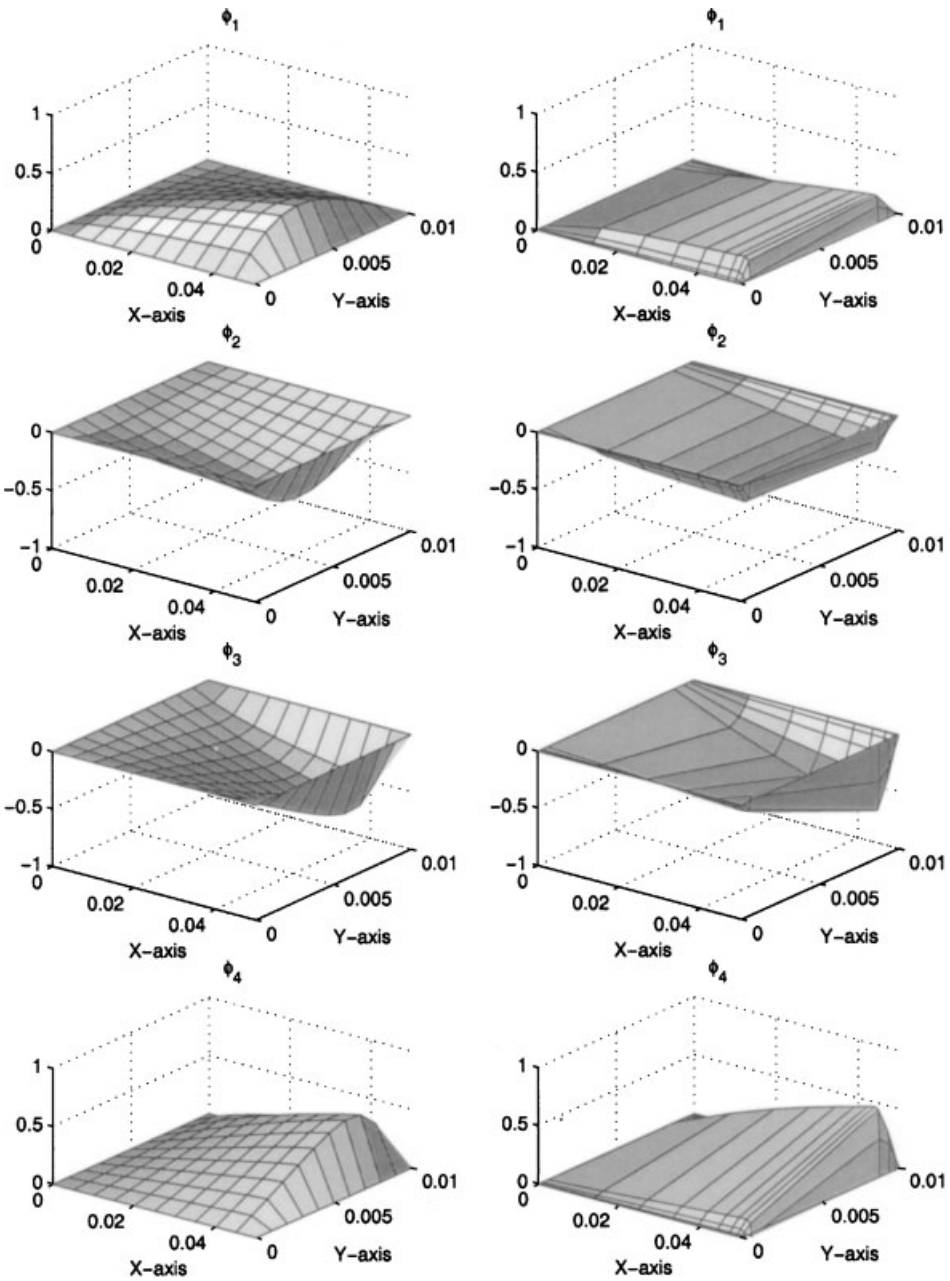

Figure 20. Bubble shape functions approximated by two different submeshes for the bottom region: uniform (left) and nonuniform (right).

Copyright © 2002 John Wiley & Sons, Ltd.

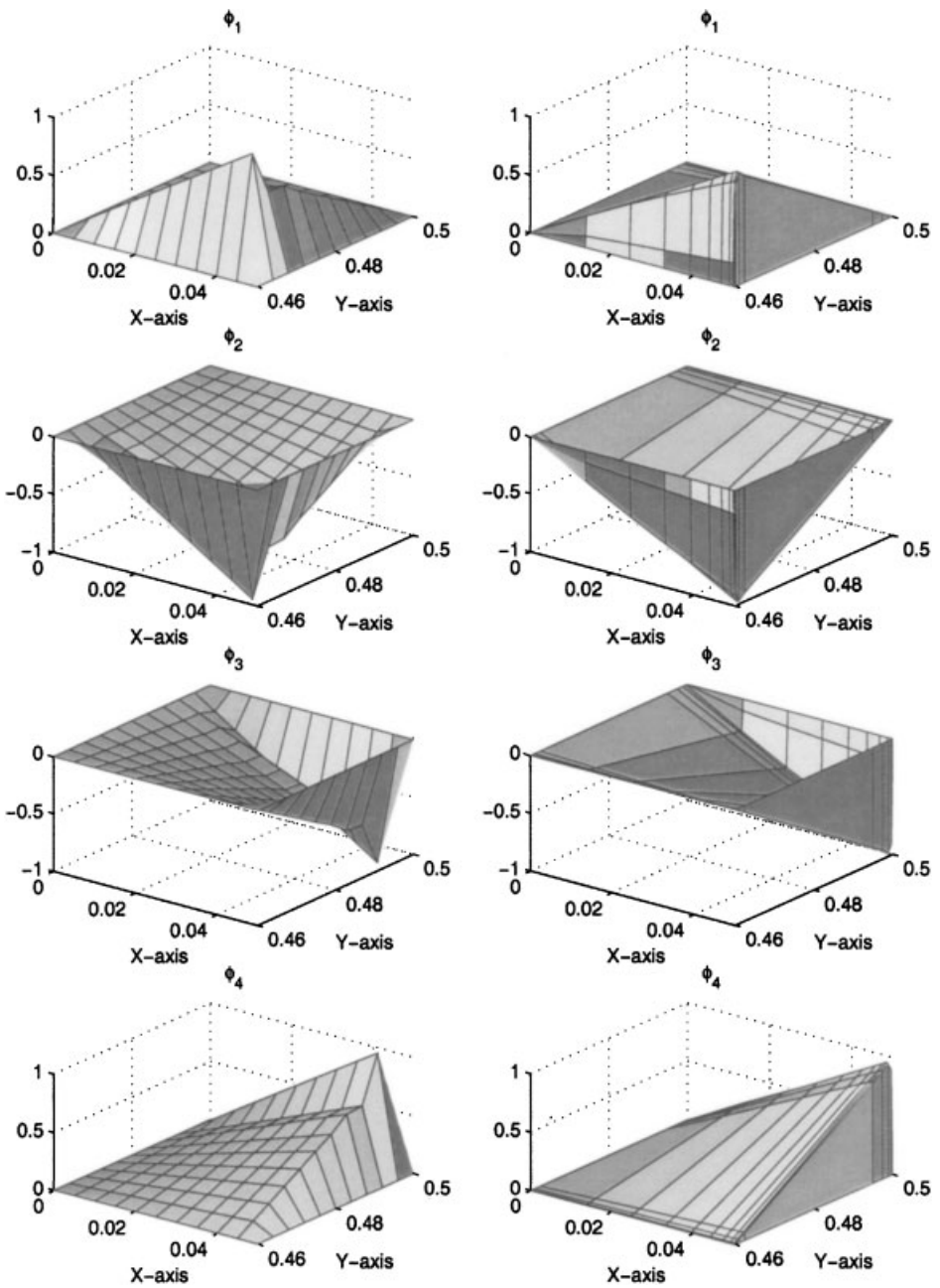

Figure 21. Bubble shape functions approximated by two different submeshes for the top region: uniform (left) and nonuniform (right).

Copyright © 2002 John Wiley & Sons, Ltd.

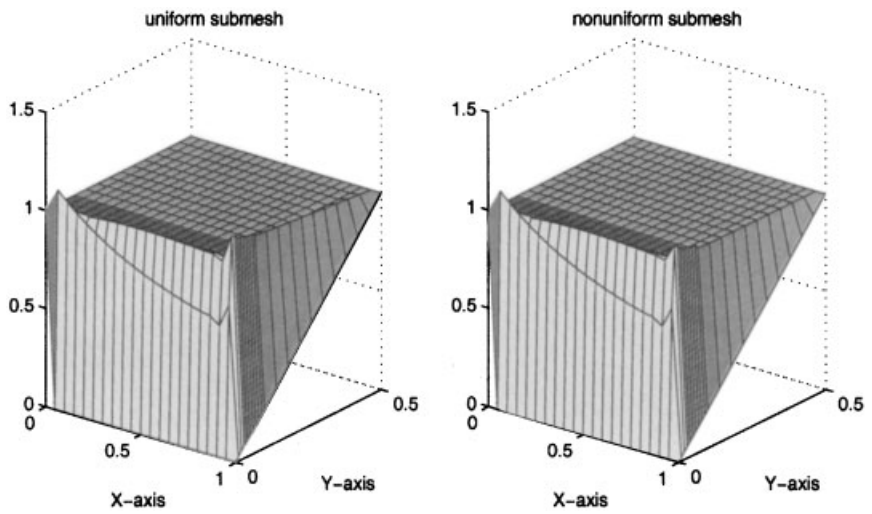

Figure 22. Comparison of the TLFEM solutions by using two different submeshes for the thermal boundary layer problem when $\kappa = 10^{-6}$: uniform (left) and nonuniform (right).

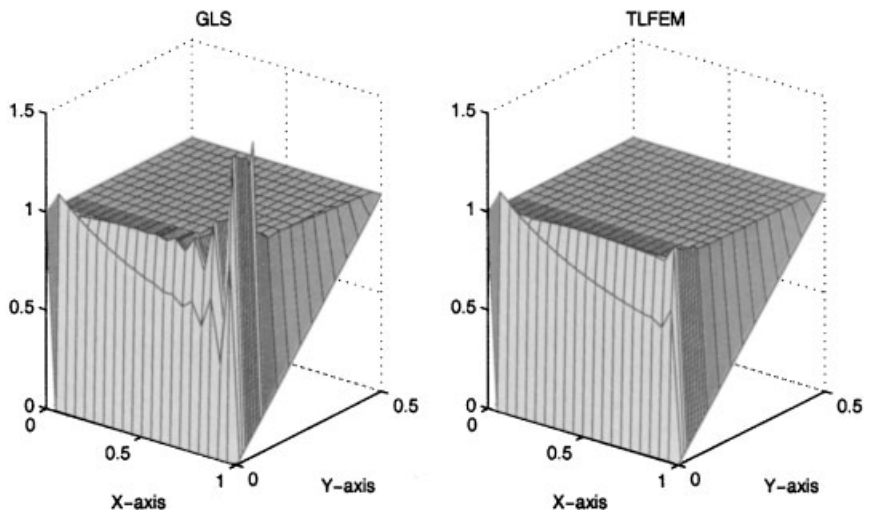

Figure 23. Comparison between the GLS method and the TLFEM method for the thermal boundary layer problem when $\kappa = 10^{-6}$: GLS (left) and TLFEM (right).

For both cases, we employ a 20×20 uniform mesh for the TLFEM and the GLS methods. First, we compare the different submesh partition strategies for the TLFEM, say 10×10 uniform submesh and nonuniform submesh (see Figure 7). For bubble shape function analysis, we pick one element to plot four shape bubble functions. The comparison of bubble shape functions by using uniform and nonuniform submesh for the 45° case is shown in Figure 8, and for 60° is shown in Figure 9. For both cases, it is obvious that nonuniform submeshes

Copyright © 2002 John Wiley & Sons, Ltd.

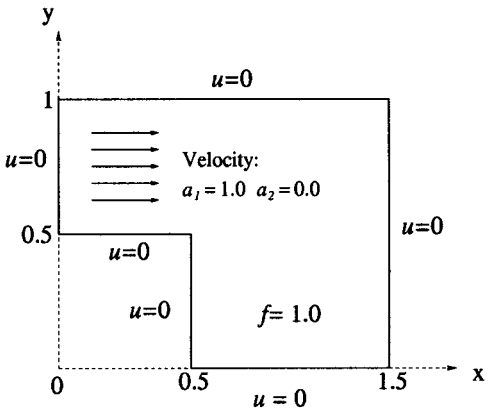

Figure 24. Problem statement for the bubble ramp problem.

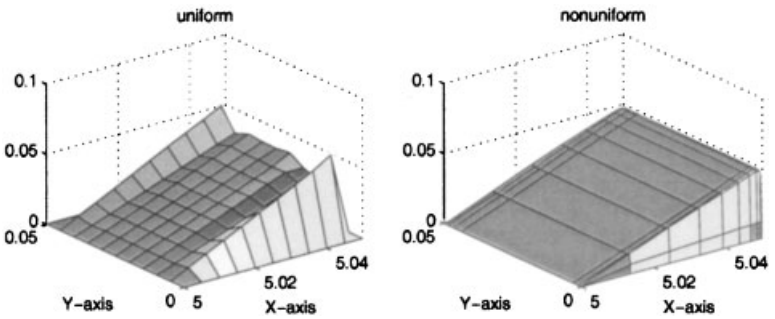

Figure 25. Comparison of bubble shape function ϕ_f by using two different submesh for the bubble ramp problem: uniform (left) and nonuniform (right).

are successful to capture the outflow boundary layers, and produce more accurate residual free shape functions. Meanwhile, the nonuniform submesh yields slightly better performance in the global solutions for both cases (see Figures 10 and 11). In Figures 12 and 13, both the TLFEM and the GLS perform similarly except in the crosswind internal boundary layer. TLFEM performs better than GLS therein.

5.2. *Thermal boundary layer problem*

Let us consider a rectangular domain of sides 1.0 and 0.5 subject to the boundary conditions presented in Figure 14. The velocity field is given by $a = (2y, 0)$ and diffusivity $\kappa = 7 \times 10^{-4}$. This problem can be viewed as the simulation of the development of a thermal boundary layer on a fully developed flow between two parallel plates, where the top plate is moving with the velocity equal to one and the bottom plate is fixed.

The non-homogeneous mesh for GLS and TLFEM methods consists of 21 equally spaced nodes in the x-direction, 11 nodes uniformly distributed in the interval $[0, 0.1]$ and 11 nodes equally spaced on $[0.1, 0.5]$ in the y-direction (see Figure 15).

Copyright © 2002 John Wiley & Sons, Ltd.

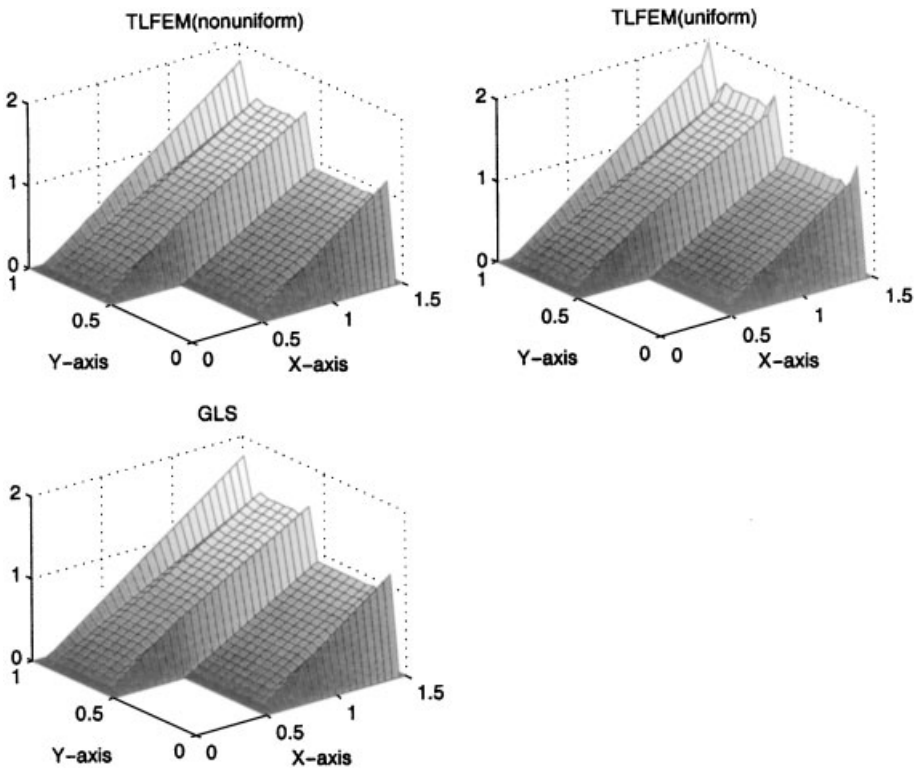

Figure 26. Comparison of the GLS and the TLFEM by using two different submeshes for the bubble ramp problem.

We wish to compare TLFEM by using the different submeshes, say 10×10 uniform and nonuniform submesh (see Figure 16).

Because the flow velocity increases along the y-direction, the solution can be divided into two regions: for the bottom of the domain, we have a diffusive dominated case; for the top of the domain, we have the advective dominated case.

We find out that the uniform submesh performs better than the nonuniform mesh for the diffusive dominated case. On the other hand, the nonuniform submesh still does a good job for the advective dominated case (see Figures 17 and 18). The global solutions for the two different submeshes are almost the same (see Figure 19).

Next we change to a smaller diffusivity $\kappa = 10^{-6}$ and rerun TLFEM by using the same meshes and submeshes and compare it with the GLS method (see Figures 20 and 21 for the bubble shape functions comparison). Taking the top plate velocity as the characteristic flow velocity, we have the mesh-Peclet number $Pe = [(|\boldsymbol{a}|h)/(2\kappa)] = 25000$. This means that the entire domain is advectively dominated. The numerical results show that the nonuniform submesh performs slightly better than the uniform one (see Figure 22). Meanwhile, the TLFEM performs better than the GLS (see Figure 23). There are some oscillations near the outflow boundary.

Copyright © 2002 John Wiley & Sons, Ltd.

5.3. *Bubble ramp problem*

Now, let us consider an L-shaped domain with external source $f=1$, $\kappa=10^{-6}$, and homogeneous Dirichlet conditions depicted in Figure 24.

A uniform partition into 300 elements are employed for the global mesh and two kinds of 10×10 submeshes are used for TLFEM. Because of the presence of the external force, the additional residual-free bubble shape function ϕ_f needs to be determined. The comparison of these approximated solutions using two different submeshes are shown in Figure 25, where the nonuniform submesh performs better than the uniform one.

The solution exhibits a strong outflow boundary layer along $x=1.5$, two crosswind boundary layers along $y=1$ and $y=0$, and a crosswind internal layer along $y=0.5$. Thus, it is one of the most stringent tests for the advective–diffusive problem. We find out that there are some improvements near the outflow boundaries in the numerical solutions for the TLFEM due to the new submesh we chose. Meanwhile, the numerical results of the GLS and the TLFEM using nonuniform submeshes are almost indistinguishable (see Figure 26).

6. CONCLUSION

In this work, we formulated the two-level finite element method based on the standard Galerkin method using piecewise linears in the original mesh, and the usual stabilized finite element method was used to approximate the partial differential equations governing the residual free bubble functions. Once these residual free bubble functions are determined, we can substitute them into the Galerkin formulation to improve the accuracy of the global numerical solution. The main advantage of this method is that we do not have to solve these partial differential equations analytically. Therefore, it is suitable for the finite element computation in a practical problem. Due to the choice of bubble functions, the boundary layers occur at outflow boundaries for the advective-dominated case. The new submesh strategy was introduced to capture this behavior. The numerical experiments confirm our idea that non-uniform submeshes are able to simulate the layer of residual-free bubble shape functions. The results display some improvements in the solution of the advective–diffusive problem, and the TLFEM solutions perform better than the GLS method in some cases. We note that the idea of the new submesh strategy can be applied to other problems in fluid dynamics, such as the incompressible Navier–Stokes equations. Non-uniform submesh depending on the direction of the flow can approximate the solution of the pressure term more accurately. See Reference [10] for its application.

REFERENCES

1. Brooks AN, Hughes TJR. Streamline upwind/Petrov–Galerkin formulation for convection dominated flows with particular emphasis on the incompressible Navier–Stokes equations. *Computer Methods in Applied Mechanics and Engineering* 1982; **32**:199–259.
2. Franca LP, Frey SL, Hughes TJR. Stabilized finite element methods: I. Application to advective–diffusive model. *Computer Methods in Applied Mechanics and Engineering* 1992; **95**:253–276.
3. Hughes TJR, Franca LP, Hulbert GM. A new finite element formulation for computational fluid dynamics: VIII. The Galerkin/least-squares method for advective–diffusive equations. *Computer Methods in Applied Mechanics and Engineering* 1989; **73**:173–189.

Copyright © 2002 John Wiley & Sons, Ltd.

4. Brezzi F, Bristeau MO, Franca LP, Mallet M, Roge G. A relationship between stabilized finite element methods and the Galerkin method with bubble functions. *Computer Methods in Applied Mechanics and Engineering* 1992; **96**:117–129.
5. Brezzi F, Franca LP, Russo A. Further considerations on residual-free bubbles for advective–diffusive equations. *Methods in Applied Mechanical Engineering* 1998; **166**:25–33.
6. Franca LP, Nesliturk A, Stynes M. On the stability of residual-free bubbles for convection–diffusion problems and their approximation by a two-level finite element method. *Computer Methods in Applied Mechanics and Engineering* 1998; **166**:35–49.
7. Franca LP, Macedo AP. A two-level finite element method and its application to Helmholtz equation. *International Journal for Numerical Methods in Engineering* 1998; **43**:23–32.
8. Franca LP, Valentin F. On an improved unusual stabilized finite element method for the advective–reactive–diffusive equation. *Computer Methods in Applied Mechanics and Engineering* 2000; **190**:1785–1800.
9. Hughes TJR. *The Finite Element Method*: *Linear Static and Dynamic Finite Element Analysis.* Prentice-Hall: New York, 1987.
10. Nesliturk A. Approximating the incompressible Navier–Stokes equation using a two-level finite element method. Ph.D thesis, University of Colorado at Denver, 1999.
11. Carey GF, Oden JT. *Finite Elements*: *Computational Aspects.* Prentice-Hall: New York, 1984.
12. Johnson C. *Numerical Solution of Partial Differential Equations by the Finite Element Method.* Cambridge University Press: Cambridge, 1987.

Copyright © 2002 John Wiley & Sons, Ltd.